Nanoscale

Tunable spin states in two-dimensional magnet CrI_3

Journal:	*Nanoscale*
Manuscript ID	NR-ART-04-2018-003230.R1
Article Type:	Paper
Date Submitted by the Author:	08-Jun-2018
Complete List of Authors:	Zheng, Fawei; Institute of Applied Physics and Computational Mathematics, Zhao, Jize; Lanzhou University Liu, Zheng; Tsinghua University Li, Menglei ; Chinese Academy of Engineering Physics, Center for Fusion Energy Science and Technology Zhou, Mei; Institute of Applied Physics and Computational Mathematics Zhang, Shengbai; Rensselaer Polytechnic Institute, Zhang, Ping; Institute of Applied Physics and Computational Mathematics,

Tunable spin states in two-dimensional magnet CrI_3

Fawei Zheng,[1,2,*] Jize Zhao,[1] Zheng Liu,[3] Menglei Li,[4] Mei Zhou,[1] S. B. Zhang,[2,5,†] and Ping Zhang[1,2,‡]

[1]*Institute of Applied Physics and Computational Mathematics, Beijing, 100088, China*

[2]*Beijing Computational Science Research Center, Beijing, 100193, China*

[3]*Institute for Advanced Study, Tsinghua University, Beijing 100084, China*

[4]*Department of Physics, Capital Normal University, Beijing 100048, China*

[5]*Department of Physics, Applied Physics and Astronomy, Rensselaer Polytechnic Institute, Troy, New York 12180-3590, USA*

(Dated: June 8, 2018)

Abstract

The recent discovery of ferromagnetic single-layer CrI_3 creates ample opportunities for studying fundamental properties as well as spintronic applications of atomically-thin magnets. Through first-principles calculations and model Hamiltonian simulations, here we build for the first time a substantial magnetic phase diagram under lateral strain and charge doping, two factors easily modulated in single-layer CrI_3 via substrate and gating controls. We demonstrate that both lateral strain and charge doping efficiently change the coupling between local spins and thus have unexpected effects on the magnetic properties of CrI_3. In particular, strain tunes the magnetic order and anisotropy: a compressive strain leads to a phase transition from a ferromagnetic insulator to an antiferromagnetic insulator, while a tensile strain can flip the magnetic orientation from off-plane to in-plane. Furthermore, we find that the phase transition under compressive strain is insensitive to charge doping, whereas the phase transition under tensile strain is modulated by electron doping significantly. Our predicted magnetic phase diagram and rationalized analysis enable single-layer CrI_3 an ideal system to harness both basic magnetic physics and building block for magnetoelastic applications.

* fwzheng@gmail.com

† zhangs9@rpi.edu

‡ zhang_ping@iapcm.ac.cn

Two-dimensional (2D) systems play an important role in modern condensed matter physics. For example, the successive discoveries of integer [1] and fractional [2] quantum Hall effects have introduced new physics to our community and stimulated long-term study of topological phenomena [3, 4]. Ever since the discovery of graphene [5], the family of 2D materials has been growing explosively, such as single-layer MoS_2 [6], FeSe [7], black phosphorus [8–10], etc. However, the 2D magnet, which is crucial for spintronics, is still missing until recently [11, 12].

It is well known that in a 2D system, strong fluctuations prohibit the long-range magnetic orders at finite temperature, as dictated by the Mermin-Wagner theorem [13]. Interestingly, the single-layer CrI_3 (SL-CrI_3) was recently found to be a realistic 2D magnet with a Curie temperature of 45 K [11]. The seeming contradiction could be resolved by considering that the strong spin-orbit coupling (SOC) associated with the heavy anion I^- explicitly breaks the SU(2) symmetry of the system and thus Mermin-Wagner theorem does not apply [14]. Inspite of this, a systematic theoretical study including SOC is still lacking. On the other hand, the successful experimental realization of a 2D magnet may provide an exciting new platform for the application of low-dimensional spintronics. Therefore, a deeper understanding of the intrinsic physical properties of SL-CrI_3 and proposals of practical methods to control its spin states are highly required. Strain [15–19] and charge doping [7, 20–22], two of the most natural methods, are widely used to modulate the properties of atomically thin 2D materials. They may lead to the emergence of new phases and can be used to control their phase transitions.

In this work, we extensively explore the possibility of controlling the magnetic properties of SL-CrI_3 by using strain and charge doping effects. Our main results are illustrated by a phase diagram as shown in Fig. 1(g). We find that both the interaction strength and anisotropy between spin freedoms are changed dramatically. As a consequence, new phases emerge in the phase diagram. Therefore, both the strain and charge doping effects can efficiently manipulate the spin sates of SL-CrI_3.

In our density functional theory (DFT) [23, 24] calculations, we take the SOC into account explicitly, based on which the magnetic anisotropy can be quantitatively determined. The calculations were performed by using the projected augmented wave (PAW) method [25–27] as implemented in VASP [28]. We used the Perdew-Burke-Ernzerhof (PBE) [29] type generalized gradient approximation (GGA) in the exchange-correlation functional. A plane-

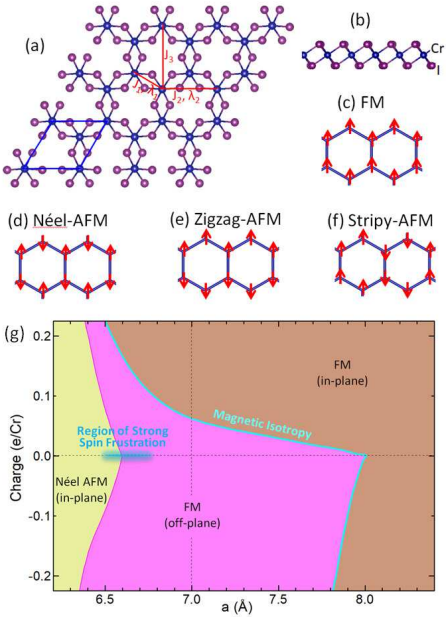

FIG. 1. (color online). (a) Top and (b) side views of SL-CrI_3 atomic structure. The blue parallelogram in (a) shows one unit cell. Different magnetic orders are shown in (c-f), where the red arrows represent the spins. The stabilites of those magnetic states are summarized in a form of phase diagram in panel (g).

wave energy cutoff of 227.1 eV was employed, which is converged in our test calculations. The Brillouin zone was sampled by 8×8×1 Monkhorst-Pack k-point mesh in primitive cell. For the case of supercell calculations, we kept the k-point density unchanged. The atomic structures were relaxed until the Feynman-Hellman force on each atoms was less than 0.01 eV/Å. Their stabilities were carefully checked by phonon dispersion calculations. Charge doping is simulated by adding or removing electrons to the CrI_3 monolayer with a compensating uniform charge background of the opposite sign. To get an accurate density of states (DOS) analysis, we also used the Wannier function techniques as coded in Wannier90 package [30].

To study the SL-CrI_3, we have adopted the slab model with the vacuum distance of 15 Å to avoid the interaction between periodical images. The atomic structure of SL-CrI_3 is plotted in Fig. 1(a,b). The Cr atoms form a honeycomb lattice. There are six I atoms forming a slightly warped octahedron around each Cr atom. The octahedron produces a crystal field, which splits the d-orbitals into t_{2g} and e_g sub-shells.

The SL-CrI_3 has been experimentally found to be ferromagnetic (FM) with an off-plane

easy axis [11]. This can be used to verify our calculation. For this purpose, we compare the total energy of the FM order with three other magnetic orders, namely Néel antiferromagnetic (Néel-AFM), zigzag anti-ferromagnetic (Zigzag-AFM), and stripy antiferromagnetic (Stripy-AFM) orders [Fig. 1(c-f)]. For all these magnetic orders, we have considered both in-plane and off-plane spin orientations. The results are summarized in Tab. I. The third column shows the total energy for SL-CrI_3 with the lattice parameter $a = 7.0$ Å, which is obtained by cell-optimization without external strain. Obviously, the off-plane FM order indeed has the lowest energy. The total energy of in-plane FM order is about 0.7 meV/Cr higher than that of off-plane FM order and others are at least 11.6 meV/Cr higher. Therefore, they are metastable states.

Since these magnetic orders are close in energy, an interesting question is whether the magnetic ground state is tunable by an external perturbation. Our DFT calculations show that the 2D Young's modulus of SL-CrI_3 is only 28 N/m, which is about one order smaller than that of graphene (340 N/m) [31] and single-layer MoS_2 (180 N/m) [32]. It is even smaller than that of single-layer FeSe (80 N/m according to our calculations). This implies that the SL-CrI_3 can be easily compressed or stretched in experiments, for example, by using the substrate lattice mismatching. It is noteworthy that the substrate-induced strain can be as large as 6% in single-layer FeSe [17, 18]. For the much softer SL-CrI_3, we expect that an even larger range of strain modulation is possible, which leaves plenty room to manipulate the spin state mechanically.

To verify our analysis, we carry out systematic calculations on the strain effect. It is well known that a 2D film such as graphene has buckling instability under compressive strain[15, 16], due to the asymmetry in tensile versus compressive strain. Nevertheless, this buckling stability in SL-CrI_3 can be largely depressed by its ultra soft feature and relatively large film-substrate interaction. In our calculations, the SL-CrI_3 is compressed to $a = 6.2$ Å at most. Our results show that the system has a magnetic phase transition from off-plane FM phase to in-plane Néel-AFM phase at $a = 6.6$ Å ($\sim$ -5.7%). For example, as shown in the second column of Table I, the total energy of in-plane Néel-AFM is 45.7 meV/Cr lower than that of off-plane FM phase, and 2.5 meV/Cr lower than that of off-plane Néel-AFM phase at $a = 6.3$ Å. Both Zigzag-AFM and Stripy-AFM orders change to other magnetic orders according to our DFT calculations. Therefore, the in-plane Néel-AFM phase is the most stable state at compressive strain condition. As for the tensile strain, the system is

stretched to $a = 8.4$ Å at most. There is also a phase transition under this condition. The system would change from off-plane FM phase to in-plane FM phase at $a = 8.0$ Å ($\sim 14.3\%$). Taking $a = 8.2$ Å for example, as shown in the fourth column of Table I, the total energy of in-plane FM is 0.2 meV lower than that of off-plane FM. The other magnetic orders are either too high in energy or unstable in our DFT calculations. Therefore, there are only three magnetic orders in the phase diagram. They are in-plane Néel-AFM, off-plane FM, and in-plane FM phases.

Furthermore, we have calculated the projected density of states (PDOS) of in-plane Néel-AFM, off-plane FM and in-plane FM phases to get the basic knowledge of their electronic structures. The electronic states near the Fermi energy are mainly composed of Cr-d orbitals mixed with some I-p orbitals. Thus, we plot the PDOS on d orbitals of a Cr atom and p orbitals of an I atom in Fig. 2. Due to the SOC effect, we can no longer divide the spins into up and down channels. However, the collinear magnetic moment orientation enables a similar expression, in which the electron spin can be along with or opposite to the polarization direction. In the cases of in-plane Néel-AFM and in-plane FM orders, the magnetic moments can be chosen along any in-plane directions and their energy differences are negligible. We choose the +x direction, and project the DOS onto I-p and Cr-d orbitals with +x and -x spin polarizations. Whereas, in the off-plane FM case, the magnetic moment

	$a = 6.3$ Å	$a = 7.0$ Å	$a = 8.2$ Å
in-plane FM	-2.6	0.7	**-0.2**
off-plane FM	0.0	**0.0**	0.0
in-plane Néel-AFM	**-45.7**	18.4	24.0
off-plane Néel-AFM	-43.2	18.5	24.9
in-plane Zigzag-AFM	–	11.6	–
off-plane Zigzag-AFM	–	11.6	–
in-plane Stripy-AFM	–	19.1	–
off-plane Stripy-AFM	–	19.1	–

TABLE I. Total energies (in meV/Cr) of SL-CrI_3 in different magnetic orders relative to the off-plane FM order. The "–"in the table means that the associated magnetic order is unstable in DFT calculations. The most stable state for each lattice parameter (a) is shown in bold font.

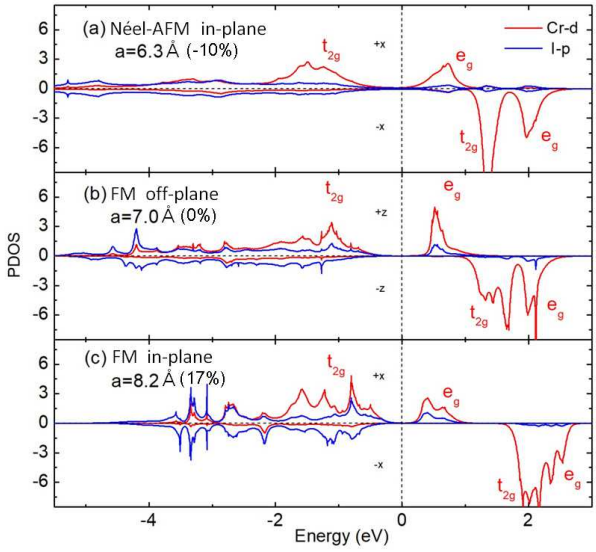

FIG. 2. (color online). PDOS for in-plane Néel-AFM (a), off-plane FM (b), and in-plane FM (c) phases. The Fermi energy is set to zero, as indicated by the black dash line.

of Cr atom is along +z direction (the off-plane direction), and the DOS is projected onto the I-p and Cr-d orbitals with +z and -z spin polarizations. The PDOS of these phases are similar. There are two groups of Cr-d peaks for +x or +z spin. One group lies below the Fermi energy, while the other group lies above the Fermi energy. There are also two groups of Cr-d peaks for -x or -z spin, but both of them stay above the Fermi energy.

We then further project these PDOS onto the five d orbitals in octahedron coordinates. The calculation results for the three magnetic orders show that, for the +x and +z spins, the Cr-d peaks below the Fermi energy are composed of d_{xy}, d_{yz}, and d_{xz} orbitals, i.e. the three t_{2g} orbitals with three electrons filling in. The other two d-orbitals belong to the e_g subshell, which accounts for the Cr-d peak above the Fermi energy. For the -x and -z spins, both t_{2g} and e_g subshells lie above the Fermi energy and are responsible for the two groups of Cr-d peaks above the Fermi energy. The calculated PDOS in Fig. 2(a-c) indicates that all the three phases are insulators. The insulating gap lies between the occupied t_{2g} levels and the empty e_g levels and thus is primarily determined by the crystal-field splitting. Our energy band calculations show that the band gap in Fig. 2(a) is 0.38 eV, which is smaller than the gap value of 0.88 eV in Fig. 2(b). When the lattice is compressed, the distances between atoms are smaller, thus the crystal field effect is stronger. It agrees with the moving trend of PDOS peaks. In Fig. 2(a), the energy difference between PDOS peaks bellow and above

the Fermi energy is larger than that in Fig. 2(b), which should have increased the band gap. While as atoms are close to each other, the overlap between their orbitals increases. As a result, the bands are spread and the band gap is effectively reduced. When the lattice is stretched, we can see that the band gap in Fig. 2 (c) is 0.65 eV, which is also smaller than that in Fig. 2(b). In this case, the larger distance between atoms weakens the crystal field and reduces the orbital overlaps. The whole effect reduces the band gap. The energy band gap and the PDOS peak positions as functions of strain and charge doping can be detected by photoemission spectroscopy and scanning tunneling spectroscopy.

To investigate the mechanism of the phase transitions induced by strain detailedly, a model Hamiltonian could be very helpful. Actually, Wang *et al.* have proposed one to explain the magnetism of SL-CrI_3 at ambient pressure [33]. They considered the first, second and third nearest neighbor Heisenberg exchange parameters and found that the first and second nearest neighbor Heisenberg exchange parameters are negative, while the third one is positive and much smaller than the former two in magnitude. This model successfully explains the ferromagnetism of SL-CrI_3 without external strain. However, it cannot explain the intrinsic magnetic anisotropy. Before long, Lado and Fernandez-Rossier proposed a nearest neighbor XXZ model [14]. They found that the anisotropy arises predominantly from the SOC in I atoms via the anisotropic symmetric superexchange. The XXZ model is capable of explaining the magnetic anisotropy at zero strain. To include the strain effect on the magnetism of SL-CrI_3, in the present work, we extend the three-neighbor Heisenberg model and the nearest neighbor XXZ model to a model Hamiltonian as,

$$\begin{aligned} H =& \sum_{nn}(J_1\vec{S_1}\cdot\vec{S_2}+\lambda_1 S_1^z S_2^z)+\sum_{2nn}(J_2\vec{S_1}\cdot\vec{S_2}+\lambda_2 S_1^z S_2^z) \\ &+\sum_{3nn} J_3\vec{S_1}\cdot\vec{S_2}\,. \end{aligned} \tag{1}$$

In this model, we consider the first, second, and third nearest neighbor Heisenberg exchange parameters, as well as the first and second anisotropy exchange parameters. As shown in Fig. 1(a), the associated Heisenberg exchange parameters are J_1, J_2, and J_3, and the anisotropy exchange parameters are λ_1 and λ_2, respectively. If we only keep λ_1 in our model Hamiltonian, the model could describe the magnetic behaviors near zero strain accurately, while it fails to explain the magnetic properties of CrI_3 under a large tensile strain. Moreover, the fitted parameter λ_1 would have very large uncertainty in the absence of λ_2. Therefore, the parameter λ_2 is indispensable. We then further test a model with λ_1, λ_2, and the third

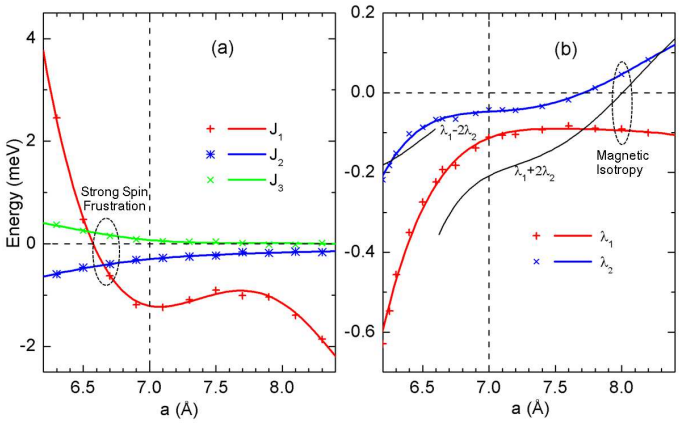

FIG. 3. (color online). The fitted (a) Heisenberg exchange parameters and (b) anisotropy exchange parameters as functions of lattice parameter.

nearest neighbor anisotropy exchange integral λ_3. The model nicely reproduces the magnetic properties of CrI_3 in the whole range of strain. However, the fitted λ_3 is at least one order smaller than λ_2, hence we can safely neglect it. In a word, a accurate and minimal model contains J_1, J_2, J_3, λ_1, and λ_2.

These parameters in our model are fitted from our DFT total energy calculations. We firstly choose a group of different spin configurations, and then calculate their total energies. After that, linear regressions are carried out to obtain the model parameters. The fitting parameters are shown in Fig. 3. The left panel shows the three Heisenberg exchange parameters. We can see that the first nearest neighbor parameter J_1 has a large amplitude and changes its sign at $a = 6.5$ Å. The parameter J_1 contains two kinds of contributions which are the direct and indirect Heisenberg exchange integrals. The Cr-Cr direct exchange integral is positive, which favors AFM. Three unpaired electrons fill the up-spin (+x or +z) t_{2g} orbitals, composing a closed shell. Due to the different symmetries, electrons from the nearest neighbor Cr atoms can not hop to the up-spin e_g orbitals. They can only hop to the down-spin t_{2g} orbitals, leading to the positive sign of the direct exchange integrals eventually. On the other hand, due to the bond angle of Cr-I-Cr which is nearly $\pi/2$, the indirect exchange integral is negative, in favor of FM orders. Therefore, the competition between the direct and indirect integrals evokes the complex behaviors of J_1. The direct integral depends on the distance between two nearest Cr atoms, which increases quickly with the decreasing of lattice parameter. Whereas, the indirect integral depends on the Cr-I

bond length as well as their relative orientations. When the SL-CrI_3 is compressed, the Cr-I-Cr angle slightly decreases, while the Cr-I bond length is barely changed. Therefore, the indirect integral is less sensitive to the lattice compression. If the system is heavily compressed, the direct integral becomes the dominant contribution. Consequently, the total integral J_1 is positive. In contrast, when the system is not heavily compressed, the indirect integral is the dominant factor, then the J_1 is negative. The second and third nearest neighbor Heisenberg exchange parameters J_2 and J_3 are also shown in Fig. 3(a). We can see that their amplitudes are relatively small and decrease with the increasing of lattice parameter. The distances from a Cr atom to its second and third nearest neighboring Cr atoms are very large (> 6 Å), thus the direct integrals are negligible. Only indirect integrals contribute to J_2 and J_3. The external strain only smoothly alters their amplitudes while keeps their signs unchanged.

The honeycomb lattice has two sub-lattices, denoted as A and B. The Heisenberg term J_2 acts within each sub-lattice. The negative sign of J_2 indicates that it is energetically favorable for atoms to align ferromagnetically within each sublattice. On the other hand, the J_3 term is always positive, preferring an antiferromagnetic configuration between the two sublattices. The J_1 term, which can be either positive or negative, determines the magnetic properties of CrI_3 crucially. In particular, for a negative J_1, there are spin frustrations between J_1 and J_3. It is highly expected that strong frustrations can lead to some exotic states of matter. In this context, CrI_3 offers a promising chance to study those nontrivial phenomena experimentally.

The fitted spin anisotropy parameter λ_1 and λ_2 are shown in Fig. 3(b). λ_1 is always negative and has relatively large amplitude. λ_2 is negative for $a < 7.2$ Å, and becomes positive for $a > 7.2$ Å. As we show in Fig. 1, each Cr atom has three nearest-neighbor Cr atoms and six second-nearest-neighbor Cr atoms. The magnetic anisotropy should be proportional to a combination of λ_1 and $2\lambda_2$. For the case of Néel-AFM phase, the anisotropy is proportional to $\lambda_1 - 2\lambda_2$. The magnetization would become off-plane when $\lambda_1 - 2\lambda_2$ is positive, and in-plane when $\lambda_1 - 2\lambda_2$ is negative. Figure 3(b) shows that the value of $\lambda_1 - 2\lambda_2$ is negative for the range of lattice parameter in Néel-AFM phase. Therefore the magnetic orientation is in-plane. For the case of FM phase, the total anisotropy is proportional to $\lambda_1 + 2\lambda_2$. The magnetization is off-plane (in-plane) for negative (positive) values of $\lambda_1 + 2\lambda_2$. From Fig. 3(b), one can see that the $\lambda_1 + 2\lambda_2$ is negative for $a < 8.0$ Å, while, it is positive

for $a > 8.0$ Å. Therefore, the system is off-plane FM for $a < 8.0$ Å, and in-plane FM for $a > 8.0$ Å. The sign change is mainly induced by the variation of λ_2, hence the phase transition at $a = 8.0$ Å is driven by the anisotropy of the second nearest neighbor exchange interaction.

To confirm the validation of our model Hamiltonian, we also perform a mean-field analysis. One hexagon ring is decoupled from the honeycomb lattice, and the surroundings are taken as effective fields. The Hamiltonian of such a cluster can be numerically diagonalized easily, and the expectation values of the spins on the cluster are readily available. These expectation values are related to the effective fields by the symmetry transformation associated with the lattice, therefore, they can be computed self-consistently. By using this method, the phases and critical points agree well with those obtained by DFT calculations as shown in Fig. 1(c). This shows that the mapping has been correctly carried out.

In addition to strain, charge doping is another common effect in epitaxial single layer. Usually, the substrate and epitaxial single layer are composed of different materials. Since they have different Fermi energies, the electrons or holes would transfer from substrate to the epitaxial layer, and vice versa. Actually, the interface-induced charge transfer has been widely used to tune the properties of epitaxial layers, such as the single-layer FeSe [7] and graphene [21, 22]. In addition, the charge doping to an ultra-thin layered material can also be introduced with the help of electrical fields or deposition atoms. For example, the potassium atoms are extensively used to dope electrons in FeSe layer [20, 34–36]. Therefore, additional charge can be easily doped to a SL-CrI_3 to tune its properties, and we also study this effect.

The effects of charge doping are demonstrated in Fig. 1(g). We can see that the AFM-FM phase transition is robust against charge doping as it can only slightly change the critical strains. The off-plane FM phase extends to the left side by a little for both the electron and hole dopings. Therefore, both charge dopings stabilize the FM phase, which is in agreement with the previous study on the energy difference between FM and AFM SL-CrI_3 without strain [33]. The phase transition between in-plane and off-plane FM phases in Fig. 1(g) behaves rather differently. Specially, the hole doping only slightly pushes the phase boundary between in-plane and off-plane FM phases to the left side, while the electron doping dramatically pushes the phase boundary to the left. Under a certain electron doping, the phase boundary crosses the vertical line at 7 Å. The crossing point locates at 0.06 e/Cr, which is not very large comparing to the doping density in single-layer FeSe experiments

[20, 34, 35]. Therefore, the charge doping can also be used to efficiently tune the magnetic anisotropy and spin orientation in SL-CrI_3.

The main results of this work are the phase transitions induced by strain and charge doping. We expect that these results can be checked by magneto-optic Kerr effect (MOKE) experiment[11]. Actually, the off-plane ferromagnetic feature of SL-CrI_3 at neutral and zero strain conditions has been revealed by polar MOKE experiment. The polar MOKE would disappear if the system is changed from off-plane FM to in-plane AFM. On the other hand, if the system is changed from off-plane FM to in-plane FM, the polar MOKE would be replaced by the longitudinal MOKE. Therefore, further MOKE experiments are desired to study the responses of SL-CrI_3 to strain and charge doping.

In conclusion, we have studied the effects of strain and charge doping on SL-CrI_3. Our calculations show that SL-CrI_3 has a rich magnetic phase diagram, including a strong spin-frustration region and a magnetic isotropic line. Strain can dramatically change the coupling between local spins, and control the phase transitions between in-plane AFM, off-plane FM, and in-plane FM phases. On the other hand, charge doping, especially the hole doping, can alter the spin orientations drastically and thereby manipulate spin states. Considering the continuously tunable nature of strain and charge doping in experiment, our present findings on extraordinarily strong couplings of spin with strain and electron doping enable the SL-CrI_3 to be a convenient platform for the study of spin frustration and Mermin-Wagner theorem, as well as a promising building block for spintronics.

[1] Klitzing, K. V.; Dorda, G.; Pepper, M. *Phys. Rev. Lett.* **1980**, 45, 494.

[2] Tsui, D. C.; Stormer, H. L.; Gossard, A. C. *Phys. Rev. Lett.* **1982**, 48, 1559.

[3] Hasan, M. Z.; Kane, C. L. *Rev. Mod. Phys.* **2010**, 82, 3045.

[4] Qi, X.-L.; Zhang, S.-C. *Rev. Mod. Phys.* **2011**, 83, 1057.

[5] Novoselov, K. S. *et al. Nature* **2005**, 438, 197.

[6] Radisavljevic, B.; Radenovic, A.; Brivio, J.; Giacometti, V.; Kis, A. *Nat. Nanotech.* **2011**, 6, 147.

[7] Wang, Q.-Y. *et al. Chin. Phys. Lett.* **2012**, 29, 037402.

[8] Qiao, J.; Kong, X.; Hu, Z. X.; Yang, F.; Ji, W. *Nat. Commun.* **2014**, 5, 4475.

[9] Li, L. *et al. Nat. Nanotech.* **2014**, 9, 372.

[10] Xia, F.; Wang, H.; Jia, Y. *Nat. Commun.* **2014**, 5, 4458.

[11] Huang, B. *et al. Nature* **2017**, 546, 270.

[12] Gong, C. *et al. Nature* **2017**, 546, 265.

[13] Mermin, N. D.; Wagner, H. *Phys. Rev. Lett.* **1966**, 17, 1133.

[14] Lado, J. L.; Fernandez-Rossier, J. *2D Mater.* **2017**, 4, 3.

[15] Zhang, Y. ; Liu, F. *Appl. Phys. Lett.* **2011**, 99, 241908.

[16] Si, C.; Sun, Z.; Liu, F. *Nanoscale* **2016**, 8, 3207.

[17] Zhang, P. *et al. Phys. Rev. B* **2016**, 94, 104510.

[18] Peng, R. *et al. Nat. Commun.* **2014**, 5, 5044.

[19] Zhou, M.; Duan, W.; Chen, Y.; Du, A. *Nanoscale* **2015**, 7, 15168.

[20] Miyata, Y.; Nakayama, K.; Sugawara, K.; Sato, T.; Takahashi, T. *Nat. Mat.* **2015**, 14, 775.

[21] Lee, J. E.; Ahn, G.; Shim, J.; Lee, Y. S.; Ryu, S. *Nat. Commun.* **2012**, 3, 1024.

[22] Shim, J. *et al. Nano Lett.* **2012**, 12, 648.

[23] Hohenberg, P.; Kohn, W. *Phys. Rev.* **1964**, 136, B864.

[24] Kohn, W.; Sham, L. J. *Phys. Rev.* **1965**, 140, A1133.

[25] Blöchl, P. E. *Phys. Rev. B* **1994**, 50, 17953.

[26] Kresse, G.; Joubert, D. *Phys. Rev. B* **1999**, 59, 1758.

[27] Blöchl, P. E.; Först, C. J.; Schimpl, J. *B. Mater. Sci.* **2003**, 26, 33.

[28] Kresse, G.; Furthmüller, J. *Phys. Rev. B* **1996**, 54, 11169.

[29] Perdew, J. P.; Burke, K.; Ernzerhof, M. *Phys. Rev. Lett.* **1996**, 77, 3865.

[30] Mostofi, A. A. *et al. Comput. Phys. Commun.* **2014**,185, 2309.

[31] Politano, A.; Chiarello, G. *Nano Res.* **2015**, 8, 1847.

[32] Bertolazzi, S.; Brivio, J.; Kis, A. *ACS Nano* **2011**, 5, 9703.

[33] Wang, H.; Fan, F.; Zhu, S.; Wu, H. *EuroPhys. Lett.* **2016**, 114, 47001.

[34] Song, C.-L. *et al. Phys. Rev. Lett.* **2016**, 116, 157001.

[35] Ren, M. *et al. Sci. Adv.* **2017**, 3, 1603238.

[36] Zheng, F.; Wang, L.-L.; Xue, Q.-K.; Zhang, P. *Phys. Rev. B* **2016**, 93, 075428.

Acknowledgments

This work was supported by NSFC(Grants Nos. 11474030, 11474029, and 11625415), National Basic Research Program of China (973 program, Grant No. 2015CB921103); S.B.Z

acknowledge the support by US NSF under the Grant No. EFMA-1542789; F. Z. acknowlege the support by China PFCAEP under the Grant No. YZJJLX2016010.

Author contributions

F.Z., S.B.Z. and P.Z. conceived the idea and initiated the research; F.Z. performed the DFT calculations and fitted the model Hamiltonian; J.Z. performed the mean-field calculations and model analysis; All authors analysed the data and prepared the manuscript.

Competing financial interests

The authors declare no competing financial interests.